

# The Fabrication of SeO<sub>2</sub> Nanoparticles from Cinnamon extract: Optical properties and its application

Saad Khalid Rahi<sup>1</sup>  , Rusul Adnan Al-Wardy<sup>2</sup>  , Hanan Abd Ali Thjeel Al Ogaili<sup>\*3</sup>  

<sup>1</sup> Department of Physics, College of Science, Mustansiriyah University, Baghdad, Iraq

<sup>2</sup> Department of Clinical Laboratory Science, College of Pharmacy, Mustansiriyah University, Baghdad, Iraq

<sup>3</sup> Department of Physics, College of Science, Wasit University, Wasit, Iraq

\*Corresponding Author.

Received 29/12/2022, Revised 12/07/2024, Accepted 14/07/2024, Published Online First 20/10/2024



© 2022 The Author(s). Published by College of Science for Women, University of Baghdad.

This is an open-access article distributed under the terms of the [Creative Commons Attribution 4.0 International License](https://creativecommons.org/licenses/by/4.0/), which permits unrestricted use, distribution, and reproduction in any medium, provided the original work is properly cited.

## Abstract

Nanoparticle biogenic synthesis (NP) has attained widespread interest due to its benefits such as simplicity, environmental friendliness, rapidity and cost-effectiveness. Selenium nanoparticles (SeO<sub>2</sub>NPs) were synthesized utilizing Cinnamomum verum bark extracts (CVBE) and selenium tetrachloride. In this study. XRD, TEM, UV and FTIR techniques were used to characterize the biosynthesized SeO<sub>2</sub> NPs. The crystal structure of SeO<sub>2</sub>-NPs is hexagonal as evidenced by XRD results. The crystalline size was achieved at about 24.5 nm and the TEM image showed that the diameter of SeO<sub>2</sub> was less than 100 nm with spherical and spherical-semi shapes. The effect of SeO<sub>2</sub> on antifungal and diverse types of bacteria was the subject of this investigation. SeO<sub>2</sub> inhibited Staphylococcus epidermidis activity against 23 mm and staphylococcus aureus activity against 21 mm, as well as antifungal isolates 18 mm, which was more effective than bacterial Klebsiella Sp. and Escherichia coli.

**Keywords:** Antimicrobial activity, Biosynthesis; Green route, SeO<sub>2</sub>, Staphylococcus

## Introduction

In response to the growing demand for nanotechnology in various fields, various methods may be chemical or physical for the preparation of NPs have been developed, including pulse laser ablation in liquid, milling by ball, CVD, and co-precipitation, chemical and electrochemical reduction<sup>1-4</sup>. chemical-Physical procedures, furthermore, have several defects, involving the utilization of hazardous chemicals, high costs, and the highest consumption of energy<sup>5-7</sup>. Environmental attention to the use of hazardous materials must be addressed<sup>8,9</sup>, thankfully, green technology overcomes these constraints<sup>10-12</sup>.

Nanoparticles produced at the nanoscale differ from those produced in bulk due to their distinct optical, magnetic, electrical, and chemical properties. These features are distinct due to the increase in the surface area concerning the small size. Due to specialized catalytic uses in addition to anti-microbial effective agents, NPs more active under effect the of solar light and UV have recently drawn the interest of the scientific community<sup>13, 14</sup>. Environmentally friendly technologies are required, and nanoparticles manufactured using green methods are critical<sup>1,2</sup>. Biogenic synthesis for nanoparticle syntheses has arisen as a promising field of nanotechnology that is both cost-effective and ecologically friendly<sup>13-16</sup>.

Severe bacterial and fungal infections have resulted in an increase in morbidity and death, necessitating aggressive treatment, including broad-spectrum antibiotic therapy<sup>1-3</sup>. Antibacterial drugs are frequently used to treat this condition, and the overuse of traditional antibiotics leads to antibiotic resistance, making infections extremely difficult to treat. Nano-materials are currently gaining favor as innovative antibacterial and antifungal agents, due to their huge specific surface area and to-volume ratio and unique physicochemical properties<sup>17-20</sup>. *Candida* spp. is one of the most common organisms that cause fungal infections, which usually result in hospital-acquired sepsis<sup>4,21</sup>, which has a death rate of up to 40%. Polyenes (amphotericin B), and diazoles

(fluconazole, Itraconazole and echinocandins are currently the most efficient antifungal drugs (caspofungin, micafungin and anidulafungin). However, side effects such as amphotericin B toxicity and inverse effects of some azoles, such as toxicity, medication interactions<sup>5-8</sup>, and yeast resistance to antifungal therapy<sup>9,10</sup>, are common when these antifungals are used. As a result, to avoid the above-mentioned negative effects, new effective antifungal therapy options must be found. SeO<sub>2</sub>NP<sub>2</sub> nanoparticles were made utilizing a biological synthesis technique in this study, and their antibacterial and antifungal capability was then assessed.

## Materials and Methods

### Experimental part

*Cinnamomum verum* (C.V.) bark powder was ground in an electric grinder and sieved through a 300 m size sieve. Then, 1 g powder was mixed with 100 mL DW and heated at 60 °C for 1/2 hour with constant stirring. At last, the mixture was filtered and utilized to make SeO<sub>2</sub> NPs. This reaction typically involves 2 grams of selenium tetrachloride in 100 ml of distilled water at 70°C for 60 minutes. The extract (5 mL) was then added and well mixed at 60°C for 1 hour under normal atmospheric pressure. The color change indicated that solution NPs were being synthesized. As depicted in Fig 1.

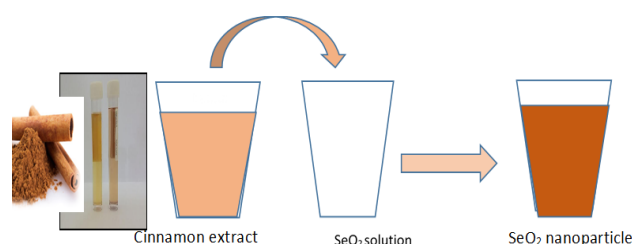


**Figure 1. Steps mixed the extract solution with SeO<sub>2</sub> solution**

## Results and Discussion

A typical XRD diffraction of SeO<sub>2</sub> produced by green synthesis and then precipitation by drop casting on glass substrate has been presented shows as Fig 2. The XRD of the nanoparticles selenium oxide indicated the summits located at  $2\theta = 24.2^\circ, 31.6^\circ, 41.8^\circ, 43.2^\circ, 45.0^\circ, 56.1^\circ, 63^\circ, 65.3^\circ$  and  $68.7^\circ$  respectively, which were typical for the selenium oxide structure. The narrow and sharp peak positions agreed with (ICDD XRD Card No. 06-0362)<sup>22</sup>. The crystalline directions (h k l) indices for nanometer-sized SeO<sub>2</sub>: (100), (101), (110), (102), (111), (003),

(202), (210) and (211) respectively for the hexagonal structure of selenium oxide crystals<sup>22,23</sup>. The average size evaluated according to Scherer Eq 1 was 24.5 nm<sup>23</sup>.

$$D = \frac{0.9\lambda}{B \cos \theta} \dots\dots\dots 1$$

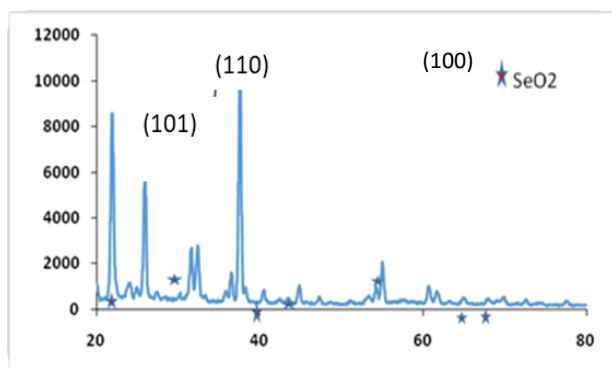


Figure 2. XRD image of SeO<sub>2</sub> nanoparticles.

TEM micrographs of SeO<sub>2</sub> NPs produced through green synthesis are shown in Fig 3. Note that the particles are either spherical or semi-spherical of the SeO<sub>2</sub> NPs, while the diameters of particles about from 4 to 22 nm, according to TEM images. It's worth noting that the average crystal diameter (24.5nm) calculated using Scherer's calculation agrees well with the value calculated using transmission electron microscope images. Both XRD and TEM give the crystal size of the material but TEM is accurate

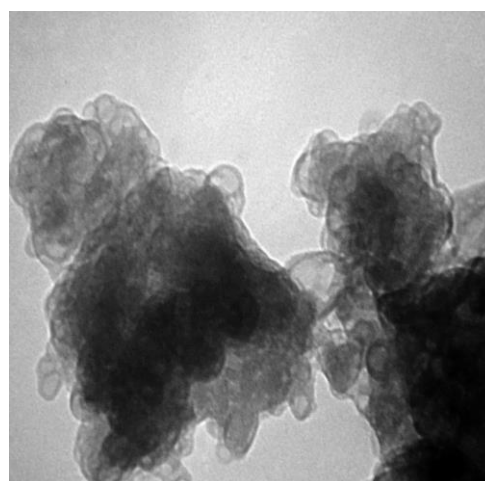
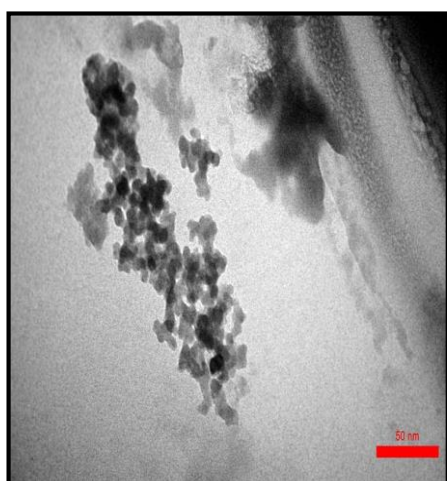


Figure 3. TEM micrographs of SeO<sub>2</sub> NPs.

Fig 4. shows the FTIR spectroscopy of produced SeO<sub>2</sub> NPs is represented by the transmission spectrum behavior of SeO<sub>2</sub>NPs in the wavelength ranging from 500 to 4500 cm<sup>-1</sup>. It's observed from the FTIR spectrum a waveband that corresponding IR and NIR wavelength ranges with the distinctive peaks refer to SeO<sub>2</sub>NPs. Depend on the previous studies found that their vibrational modes of SeO<sub>2</sub> NPs, where summits at about 597 and 732 (1/cm) specified to the vibrational modes of v<sub>2</sub> and v<sub>3</sub>, while it observed the stretching frequency at 1654 cm<sup>-1</sup> of C=O bonds. Also, hydrogen bonds that are strong molecular with (OH), amine and carboxyl groups were noticed close to the broadband between (322–3395 cm<sup>-1</sup>)<sup>22,24</sup>.

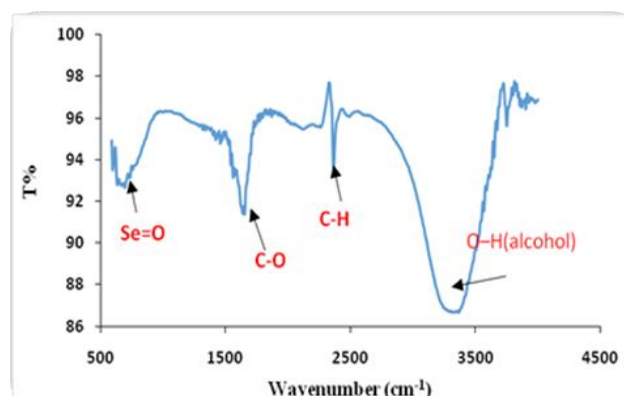
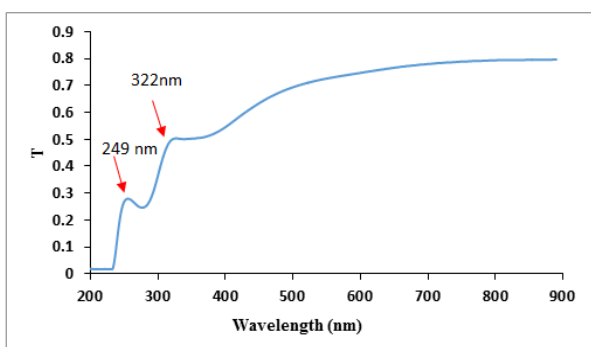


Figure 4. FTIR of SeO<sub>2</sub> NPs

The optical transmittance properties of SeO<sub>2</sub> nanoparticles are shown in Fig 5. There are two peaks at 249 nm and 322 nm observed, also, the result confirms the formation of SeO<sub>2</sub> Nanoparticles. These peaks could be attributed to the existence of two different sizes or shapes of the Nano-particles<sup>25</sup>. The sample exhibits high transparency properties in

the spectral range 460-900 nm. At wavelengths of 890 nm, SeO<sub>2</sub> NPs had a maximum transmittance of roughly 0.7 percent. It is important to understand that the properties of SeNPs depend on their size and shape. According to a recent report, SeNPs have shown numerous absorption bands at UV-vis wavelengths due to the quantum confinement effect and synthetic protocols<sup>26</sup>.



**Figure 5. UV- Visible Spectroscopy of SeO<sub>2</sub> NPs from Cinnamomum verum extract**

Fig 6: Gap optical SeO<sub>2</sub> NPs, where the plot of  $(\alpha h\nu)^2$  vs. the photon energy denoted by  $h\nu$ , and  $\alpha$  represented to (the coefficient of absorption). The band gaps of SeO<sub>2</sub> NPs were discovered to be 3.8 eV and 5.1 eV by projecting the linear component of the curve toward the photon energy axis by Tauc's model<sup>27</sup>

$$(\alpha h\nu)^2 = A (h\nu - E_g) \dots\dots 2$$

The fluctuation of the edge of absorption produced by the structure of the energy band, as well as the variation in the density of state with energy level, can explain the occurrence of a two-energy gap. The energy gap has widened, which may be belonged to the size restriction<sup>27</sup>.

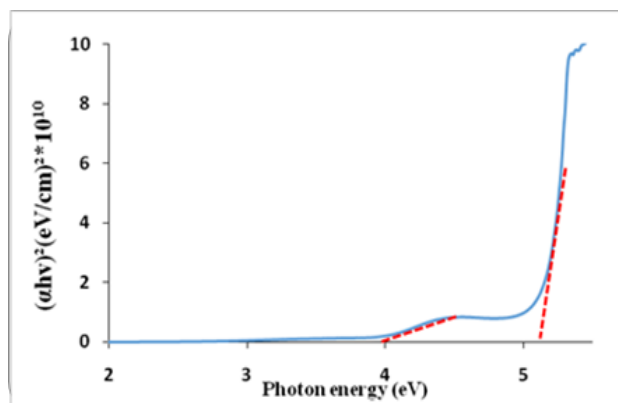


**Figure 6. Energy gaps plot of SeO<sub>2</sub> NPs**

The activity for antibacterial and anti-fungal of the synthesized SeO<sub>2</sub>NPs was tested against pathogenic organisms like (*Staphylococcus aureus*, *E. coli*, *Klebsiella Sp.*, *Candida* and *Staphylococcus epidermidis*). The strains were grown in LB broth for one day at 37°C for bacteria and 30°C for *Candida albicans* before being spread on LB agar plates with a sterile glass spreader. Following that, sterile paper discs (6mm in diameter) were placed on inoculated plates, followed by the loading of SeO<sub>2</sub> NP samples onto each disc, the inhibitions zones were utilized to measure the activity of the antibacterial and antifungal, where it formed around the discs. The *Staphylococcus epidermidis* activity against 23 mm and *Staphylococcus aureus* 21 mm was demonstrated by the plant-mediated synthesis of SeO<sub>2</sub>NPs. The results showed that SeO<sub>2</sub> NPs also have efficiency contra isolates of antifungal as in Fig 7. Also, Table1. The literature explains potential pathways for SeO<sub>2</sub> NPs' antifungal action, where the diffusion and endocytosis were routes to enter SeO<sub>2</sub> NPs to the cell, interfering with mitochondrial activity in cytoplasm contact and may cause the releasing of ROS (reactive oxygen species) and Se<sup>2+</sup>. These ions can pass through the cell membrane and then to DNA, which causes damage to DNA and cell death<sup>28</sup>. The exact mechanism of NPs mode antibacterial action is unknown at this time. It postulated three distinct mechanisms so far: I rupture of cell walls and membranes, (II) the penetration of intracellular then the damage, also (III) the oxidative stress<sup>29-34</sup>. SeO<sub>2</sub> NPs' antifungal action is mediated by nanoparticles and is dependent on ROS.

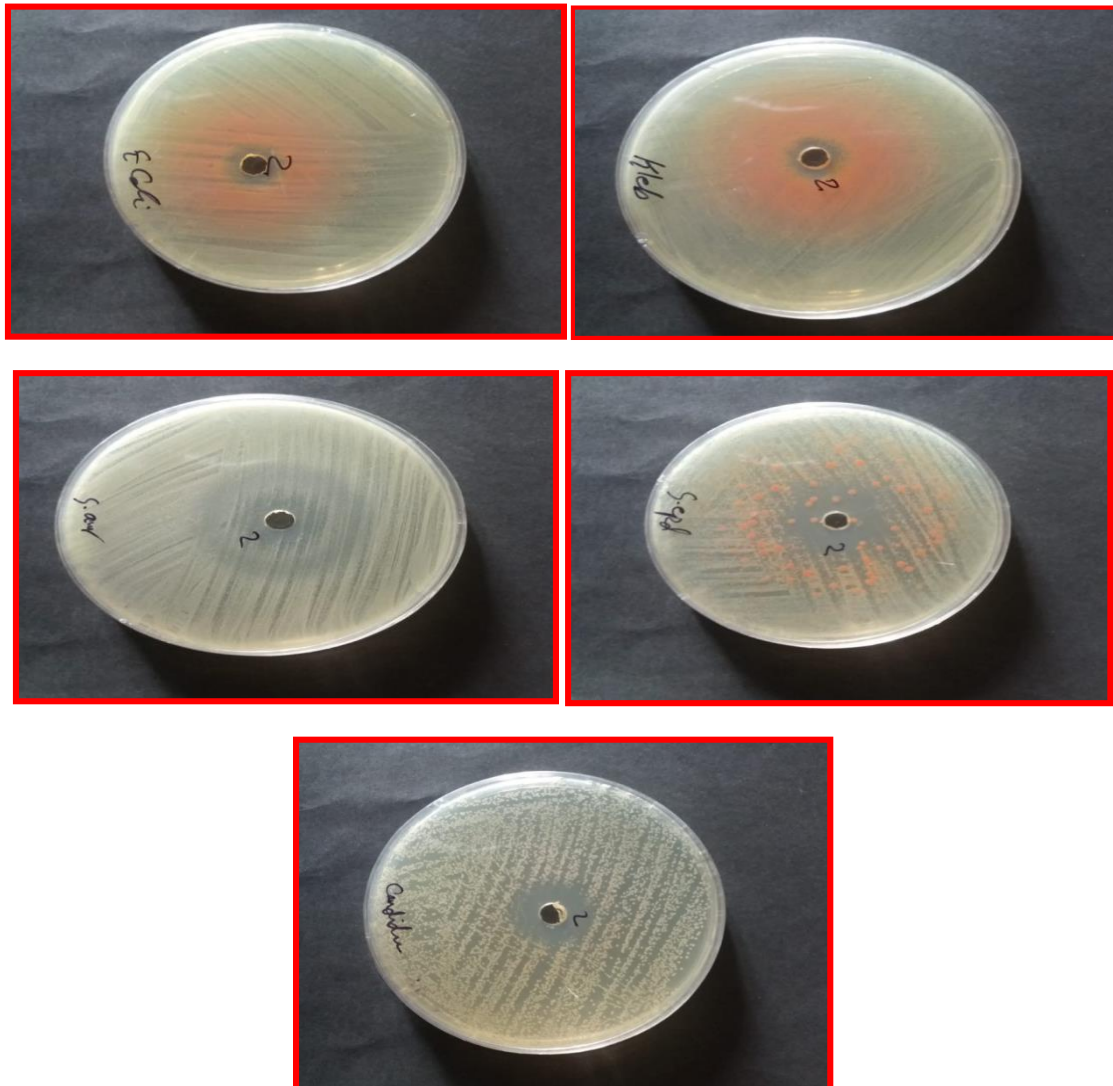


**Figure 7. Activity of selenium oxide NPs contra anti-bacterial and anti-fungal**

**Table 1. Activity of selenium oxide NPs contra anti-bacterial and anti-fungal**

<b>Klebsiella sp.(gram –ve)</b>	<b>E-coli(gram – ve)</b>	<b>Staphylococcaa aureus (gram+ve)</b>	<b>Staphylococcaa Epidermidis(gram +ve)</b>	<b>candida</b>
<b>11mm</b>	10mm	21mm	23mm	18mm

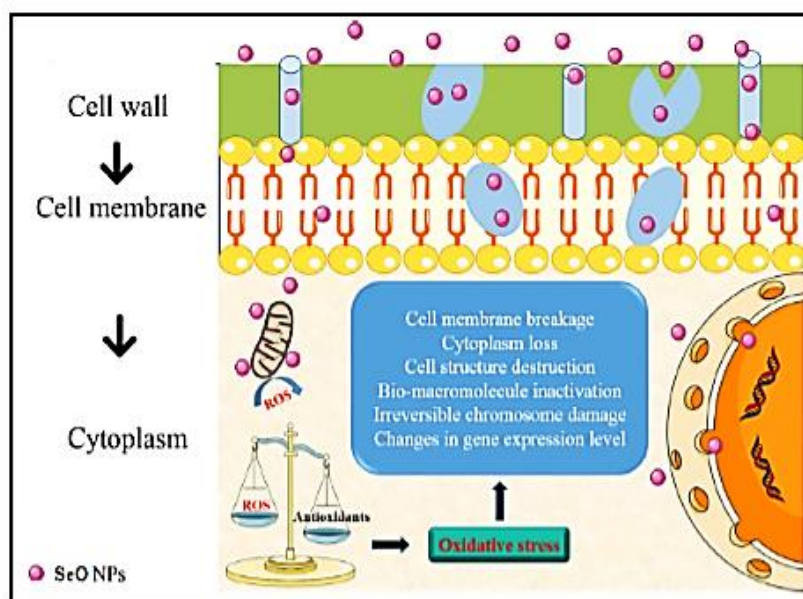


**Figure 8. ROS produced by SeO<sub>2</sub>NPs - depending on the antifungal activity**

## Conclusion

(SeO<sub>2</sub>NP<sub>s</sub>) were made utilizing Cinnamomum verum bark extracts (CVBE) and selenium tetrachloride as a Se precursor in this study. XRD, TEM, FT-IR, and UV-Vis routes were utilized to characterize the biosynthesized SeO<sub>2</sub>NPs. The average crystalline size of SeO<sub>2</sub>NPs was 24.5 nm. Images of TEM illustrated that the SeO<sub>2</sub> NPs were

spherical and semi-spherical in shape with a diameter between 4nm to 22 nm. Results revealed the plant-mediated synthesis of SeO<sub>2</sub>NPs exhibited good Staphylococcus epidermidis activity against 23 mm and Staphylococcus aureus 21 mm, as well as efficiency against isolates of anti-fungal 18 mm.

## Authors' Declaration

- Conflicts of Interest: None.
- We hereby confirm that all the Figures and Tables in the manuscript are ours. Furthermore, any Figures and images, that are not ours, have been included with the necessary permission for re-publication, which is attached to the manuscript.
- No animal studies are present in the manuscript.
- No human studies are present in the manuscript.
- Ethical Clearance: The project was approved by the local ethical committee at Mustansiriyah University.

## Authors' Contribution Statement

S K and R A conceived of the presented idea S K designed, developed the theory and performed the computations R A , and SK verified the analytical methods. SK and H A J Encouraged H A to investigate Algorithms and compare different

approaches related to service problem in future networks . HA and RA supervised the findings of this work. the authors write the article be careful and the results were discussed, and contributed to the final manuscript

## References

1. Bibi I, Kamal S, Ahmed A, Iqbal M, Nouren S, Jilani K, et al. Nickel nanoparticle synthesis using *Camellia Sinensis* as reducing and capping agent: Growth mechanism and photo-catalytic activity evaluation. *Int J Biol Macromole.* 2017; 103: 783-790. <https://doi.org/10.1016/j.ijbiomac.2017.05.023>
2. Abed FG, Jubeir NJ, Al Ogailli HAT. Study Effect of the concentration of Iron on the Synthesized Zinc Oxide via the plant extract of beetroot. *AIP Conf Proc.* 2024; 2922(1): 040006 <https://doi.org/10.1063/5.0183132>
3. Alijani H Q, Pourseyedi S, Mahani M T, Khatami M. Green synthesis of zinc sulfide (ZnS) nanoparticles using *Stevia rebaudiana* Bertoni and evaluation of its cytotoxic properties. *J Mol Struct.* 2019; 1175: 214-218. <https://doi.org/10.1016/j.molstruc.2018.07.103>
4. Nava O J, Luque PA, Gómez-Gutiérrez C.M., Vilchis-Nestor A.R., Castro-Beltrán A., Mota-González M., et.al. Influence of *Camellia sinensis* extract on Zinc Oxide nanoparticle green synthesis. *J Mol Struct.* 2017; 1134: 121-125. <https://doi.org/10.1016/j.molstruc.2016.12.069>
5. Reddy K.R., Green synthesis, morphological and optical studies of CuO nanoparticles. *J Mol Struct.* 2017; 1150: 553-557. <https://doi.org/10.1016/j.molstruc.2017.09.005>
6. Sabouri Z, Akbari A, Hosseini H A, Darroudi M. Facile green synthesis of NiO nanoparticles and investigation of dye degradation and cytotoxicity effects. *J Mol Struct.* 2018; 1173: 931-936. <https://doi.org/10.1016/j.molstruc.2018.07.063>
7. Arshad M, Hussain T, Iqbal M, Abbas M. Enhanced ethanol production at commercial scale from molasses using high gravity technology by mutant *S. cerevisiae*. *Brazil J Microbiol.* 2017; 48. <https://doi.org/10.1016/j.bjm.2017.02.003>
8. Arshad M, Qayyum A A G, Haider R. Iqbal M, Nazir A. Influence of different solvents on portrayal and photocatalytic activity of tin-doped zinc oxide nanoparticles. *J Mol Liq.* 2018; 260:272-278. <https://doi.org/10.1016/J.MOLLIQ.2018.03.074>
9. Ashar A, Iqbal M, Bhatti IA, Ahmad MZ, Qureshi K, Nisar J, et al. Synthesis, 318 characterization and photocatalytic activity of ZnO flower and pseudo-sphere: Nonylphenol 319 ethoxylate degradation under UV and solar irradiation. *J Alloy Comp.* 2016; 678: 126-136. <http://dx.doi.org/10.1016%2Fj.jallcom.2016.03.251>
10. Shahab-ud-Din, Ahmad MZ, Qureshi K, Bhatti IA, Zahid M, Nisar J ,etal . Hydrothermal synthesis of molybdenum trioxide, characterization and photocatalytic activity. *Mater Res Bull.* 2018; 100: 120-130. <https://doi.org/10.1021/jp0684628>.
11. Nazar N, Bibi I, Kamal S, Iqbal M, Nouren S, Jalani K, et al. Cu nanoparticles synthesis using a biological molecule of *P. granatum* seeds extract as reducing and capping agent: Growth mechanism and photo-catalytic activity. *Int J Biol Macromol.* 2017; 106: 326. <https://doi.org/10.1016/j.molliq.2018.02.034>
12. Igwe OU, Nwamezie F. Green synthesis of iron nanoparticles using flower extract of *Piliostigma thonningii* and the antibacterial activity evaluation. *Chem Int.* 2018; 4: 60-66. <http://www.bosaljournals/chemint/>
13. Prabu H J, Johnson I. Plant-mediated biosynthesis and characterization of silver nanoparticles by leaf extracts of *Tragia involucrata*, *Cymbopogon citronella*, *Solanum verbascifolium* and *Tylophora ovata*. *Karbala Int J Modern Sci.* 2015; 1: 237-246. <https://doi.org/10.1016/j.kijoms.2015.12.003>
14. Kahrilas GA, Wally LM, Fredrick SJ, Hiskey M, Prieto AL, Owens JE. Microwave assisted green synthesis of silver nanoparticles using orange peel extract. *ACS Sustain Chem Eng.* 2013; 2: 367-376. <https://doi.org/10.1021/sc4003664>.
15. Aragão AP, de Oliveira TM, Quelemes PV, Perfeito MLG, Araújo MC, Santiago JD ,et al. Green synthesis of silver nanoparticles using the seaweed *Gracilaria birdiae* and their antibacterial activity. *Arab J Chem.* 2016 12(1): 4182-4188. <http://dx.doi.org/10.1016/j.arabjc.2016.04.014>
16. Ahmed S, Ahmad M, Swami B L, Ikram S. A review on plants extract mediated synthesis of silver nanoparticles for antimicrobial applications: A green expertise. *J Adv Res.* 2016; 7: 17-28 <https://doi.org/10.1016/j.jare.2015.02.007>
17. Huh AJ, Kwon YJ. Nano antibiotics: A new paradigm for treating infectious diseases using nanomaterials in the antibiotics resistant era. *J Control. Release.* 2011; 156: 128-145. <https://doi.org/10.1016/j.jconrel.2011.07.002>
18. Li W, Dong K, Ren J, Qu X. A Lactamase-imprinted responsive hydrogel for the treatment of antibiotic-resistant bacteria. *Angew Chem Int Ed Engl.* 2016; 55 (28): 8049–8053. <https://doi.org/10.1002/anie.201600205>
19. Fan W, Tong Farn X, Yu B, Zhao Y. CO<sub>2</sub>-responsive polymer single-chain nanoparticles and self-assembly for gas-tunable nanoreactors. *Chem Mater.* 2017; 29: 5693–5701. <https://doi.org/10.1021/acs.chemmater.7b01656>
20. Wu Y, Song Z, Wang H, Han H., Endogenous stimulus-powered antibiotic release from nanoreactors for a combination therapy of bacterial infections. *Nat Commun.* 2019; 10: 1–10. <https://doi.org/10.1038/s41467-019-12233-2>
21. Ales Panáček, Milan K , Renata V, Robert P, Jana S, et al. Antifungal activity of silver nanoparticle against *Candida* spp. *Biomaterials.* 2009; 30: 6333–6340. <https://doi.org/10.1016/j.biomaterials.2009.07.065>
22. Monireh K, Alireza A, Hossein Z, Saman S, Zahra S. Mehrdad K, et al. Evaluation of Antifungal and

- Photocatalytic Activities of Gelatin-Stabilized Selenium Oxide Nanoparticles. *J Inorg Organomet Polym Mater.* 2020; 30(38): 3036–3044. <https://link.springer.com/article/10.1007/s10904-020-01462-4>
23. Soumya M, Venkat K S. Cytotoxicity Analysis of Biosynthesized Selenium Nanoparticles Towards a Lung Cancer Cell Line. *J Inorg Organomet Polym Mater.* 2019; 30(4): 1852–1864. <https://link.springer.com/article/10.1007/s10904-019-01409-4>
24. Vetrivel C, Durairaj K, Kalaimurugan D, Viji M, Muruges E, Wen C L, et al. Green synthesis of selenium nanoparticles mediated from *Ceropegia bulbosa* Roxb extract and its cytotoxicity, antimicrobial, mosquitocidal and photocatalytic activities. *Sci Rep.* 2021; 11: 1032 <https://doi.org/10.1038/s41598-020-80327-9>
25. Rahi S K, Hassoni M H, Abd A N. Study effect of reinforcement and moisture on the impact strength of hybrid and single polymeric composites. *J Eng applied Sci.* 2018; 13(18): 7624–7629 <http://dx.doi.org/10.36478/jeasci.2018.7624.7629>
26. Hassanien R, Abed- Elmageed AA, Husein DZ. Eco-Friendly Approach to Synthesize Selenium Nanoparticles: Photocatalytic Degradation of Sunset Yellow Azo Dye and Anticancer Activity. *Chem Sel.* 2019; 4(31): 9018-9026. <https://doi.org/10.1002/SLCT.201901267>
27. Abbas SI, Thjeel Al Ogaili HAA. Nonlinear optical characteristics of chemical bath-deposited pure and Cu-doped SnO<sub>2</sub> thin films: A comparative evaluation. *Resu. Opt..* 2023; 13: 100529 <https://doi.org/10.1016/j.rjo.2023.100529>
28. Maria S J, Joseph A N, Kesava P R, Alessio M, Gabriele G, Antonino Natalello, et al. Synthesis of Bioactive Silver Nanoparticles by a *Pseudomonas* Strain Associated with the Antarctic Psychrophilic Protozoan *Euplotes focardii*. *Mar Drugs.* 2020; 18(38): 1-13. <http://dx.doi.org/10.3390/md18010038>
29. Al -Ogaili HAT, Al-Wardy RA. Thermal analysis for stability the nanocrystals ZnSe(diamantane) *J Phys: Conf Ser.* 2020; 1591(1): 012008 <https://doi.org/10.1088/1742-6596/1591/1/012008>
30. Abd A N, Abdullah M T, Rahi S K, Habubi N F. CdO/FTO Schottky photodetector with enhanced spectral responsivity and Specific detectivity prepared by electrolysis method. *J Phys: Conf Ser.* 2020; 1660(1): 012047. <https://doi.org/10.1088/1742-6596/1660/1/012047>
31. Rahi S K, Hahamd W I, Thakir H N. Influence of the thermal annealing on properties of cadmium sulfide: Copper 10% thin films and solar cell application. *Mater Today Proc.* 2021; 47: 6192-6196. <https://doi.org/10.1016/j.matpr.2021.05.15>
32. Zainab J S, Sabah M H, Sabeeha K S. Structural Analysis of Chemical and Green Synthesis of CuO Nanoparticles and their Effect on Biofilm. *Baghdad Sci J.* 2018; 15(2): 211. <http://dx.doi.org/10.21123/bsj.2018.15.2.0211>
33. Al Ogaili HAT, Abbas SI, Mohammed M A. Raman spectra and electronic features for nanotubes of znse wurtziod: Ab-initio. *Chalcogenide Lett.* 2020; 17(5): 251–255. [https://chalcogen.ro/251\\_OgailiHAT.pdf](https://chalcogen.ro/251_OgailiHAT.pdf)
34. Ahmed K H, Mohammed A A , Imad ML. A Green Synthesis of Iron/Copper Nanoparticles as a Catalytic of Fenton-like Reactions for Removal of Orange G Dye. *Baghdad Sci J.* 2022; 19(6): 6508. <https://dx.doi.org/10.21123>



## تصنيع الجسيمات النانوية لأكسيد السليسيوم من مستخلص القرفة: خصائصه البصرية وتطبيقاته

سعد خالد راهي<sup>1</sup>، رسل عدنان الوردى<sup>2</sup>، حنان عبدعلي ثجيل العكيلي<sup>3</sup>

<sup>1</sup> قسم الفيزياء، كلية العلوم، الجامعة المستنصرية، بغداد، العراق.

<sup>2</sup> قسم المختبرات السريرية، كلية الصيدلة، الجامعة المستنصرية، بغداد، العراق

<sup>3</sup> قسم الفيزياء، كلية العلوم، جامعة واسط، واسط، العراق

### الخلاصة

حظي التصنيع الحيوي للجسيمات النانوية باهتمام واسع النطاق بسبب فوائده مثل البساطة والملائمة للبيئة والسرعة والفعالية من حيث التكلفة. تم تصنيع جسيمات السليسيوم النانوية (SeO<sub>2</sub>NPs) باستخدام مستخلصات لحاء القرفة (CVBE) ورباعي كلوريد السليسيوم. في هذه الدراسة، تم استخدام تقنيات XRD و TEM و UV و FTIR لتوصيف SeO<sub>2</sub> NPs المُصنَّع بيولوجيًا، البنية البلورية لها تكون سداسية كما يتضح من نتائج الأشعة السينية. تم تحقيق الحجم البلوري حوالي 24.5 نانومتر وأظهرت صورة TEM أن قطر SeO<sub>2</sub> كان أقل من 100 نانومتر بشكل كروي وشبه كروي. كان تأثير SeO<sub>2</sub> على مضادات الفطريات وأنواع مختلفة من البكتيريا موضوع هذا البحث. SeO<sub>2</sub> كمثبط لنشاط المكورات العنقودية مقابل 23 ملم ونشاط المكورات العنقودية الذهبية مقابل 21 ملم، وكذلك العزلات المضادة للفطريات 18 ملم، والتي كانت أكثر فعالية من البكتيرية Klebsiella Sp. والإشريكية القولونية.

**الكلمات المفتاحية:** الفعالية ضد المايكروبات – التصنيع الحيوي – الطريقة الخضراء – أكسيد السليسيوم – الإشريكية القولونية.